Automated Recognition of Type III Solar Radio Bursts using Mathematical Morphology

James C. Jones
Northrop Grumman
Dr. Gregory P. Richards
Northrop Grumman

CONFERENCE PAPER

Modern technology, specifically radio communications, is particularly vulnerable to various aspects of space weather. The solar environment can disrupt satellite communication links which can have a variety of impacts from loss of data to loss of spacecraft control. Radio spectrograph instruments are used to monitor the sun's coronal emissions of plasma that travel with the solar wind towards Earth. These radio bursts are detected by radio observatories around the world, analyzed manually, and bulletins are created to notify satellite operators. This paper presents a real-time method to automatically detect and classify radio bursts measured by solar radio spectrographs using mathematical morphology, which is ideal for the identification of shapes or objects embedded in complex backgrounds. Since type III radio bursts typically last only about one to three seconds they have a distinctive shape, a vertical line that spans a wide frequency range in a short time period, the object can be detected with a single structuring element. Data from the current solar max were used to validate the method. Results were compared to the manual analysis from the observatories.

1. INTRODUCTION

The Sun is a significant source of radio emissions which indicate various phenomena related to solar activity. Continuous levels of radio wave emission are observed at the 10.7 cm wavelength contributing to the $F_{10.7}$ index commonly used to initialize space weather models [1]. The $F_{10.7}$ index is a good indicator of long term solar activity trends such as the solar cycle. More sporadic emissions are routinely measured by solar radio spectrographs (SRS) and are categorized by their characteristics as measured by these instruments. These sporadic emissions are grouped into four types: I, II, III, and IV [2]. Type I events, or noise storms, are characterized by numerous intense, sharp bursts originating near sunspots. These noise storms can last for hours to days. Type II bursts last from 5 to 30 minutes and typically occur in conjunction with solar flares. Type III bursts consist of short duration (on the order of seconds) bursts and occur generally at the start of solar flares. The Type IV bursts are of long duration and are related to proton emission and expanding magnetic field lines.

The focus of this work is on the automated detection of Type III radio bursts. The physical mechanism causing these types of bursts is related to energized electrons propagating along magnetic field lines in the solar corona. Higher energy electrons can overtake lower energy electrons which causes an acceleration (often called a bump or beam) in the forward direction of the bulk plasma. This causes instability that can resonate and generate Langmuir waves which undergo non-linear wave-wave interaction and produce electromagnetic emissions at the local electron plasma frequency and the second harmonic of this frequency. As these beams escape upward into interplanetary space, away from the solar corona, they encounter decreasing plasma

density which results in a decrease in the radio frequency which gives the Type III bursts their characteristic decrease in frequency with time [3].

The significance of these radio bursts depends on the frequencies they generate and the frequencies of the communication systems in use. It has been shown in [4] how solar radio bursts can impact radio communications and precision navigation and timing. Kennewell and McDonald documented a case in which radio noise bursts associated with an X-class flare caused loss of lock with GPS satellites for 2 hours [5]. Sreeja et al. associated a solar radio burst with the loss of Global Navigation Satellite System (GNSS) signal by receivers and therefore a reduction in positioning accuracy [6]. Interference to cell phone networks and other wireless systems resulting in dropped calls has been shown by Gary et al. [7]. Ralston et al. have shown how radio bursts contribute to the noise temperature of VHF and UHF radar [8]. Oftentimes negative effects on systems go unreported since the ability of the sun to impact systems is not well known to system operators and tend to be transitory in nature. Therefore it is imperative to monitor frequencies used for critical defense needs to fully comprehend the source of system malfunctions.

2. THE US AIR FORCE SOLAR RADIO SPECTROGRAPH

The US Air Force operates a network of solar radio observatories around the world. These sites include: the Sagamore Hill Solar Observatory near Boston, Mass., the Kaena Point Solar Observatory on Oahu, Ha., the Learmonth Solar Observatory in Western Australia, and the San Vito Solar Observatory in Italy. These observatories have a variety of instrumentation and in particular host solar radio spectrographs that monitor the sun from 25 to 180 MHz. The SRS instruments are composed of two separate systems across two bands: 25-75 MHz, or Low Band, and 75-180 MHz, High Band. Each band is separated into 401 subbands. The instrument sweeps across the full band (25 to 180 MHz, 802 subbands) every three seconds. The signal intensity in each subband is measured on a relative logarithmic scale and assigned an integer from 0 to 255. The data are then presented on a display screen to the on-site analyst who monitors the data and sends reports when radio bursts occur. Manual analysis has been the method employed to report solar radio bursts detected at USAF sites for decades.

The USAF sites have recently undergone a slight modernization to digitize the SRS measurements and return the data to the Air Force Weather Agency (AFWA) in Omaha, Ne. These data are bundled in one-minute blocks and transferred via the internet to AFWA where they are collected, processed, displayed, and stored. This modernization effort has delivered the ability to share data between observatories and allow AFWA scientists to analyze the SRS data and develop automated recognition algorithms. The following image shows an example of the real time viewer of the SRS at Sagamore Hill.

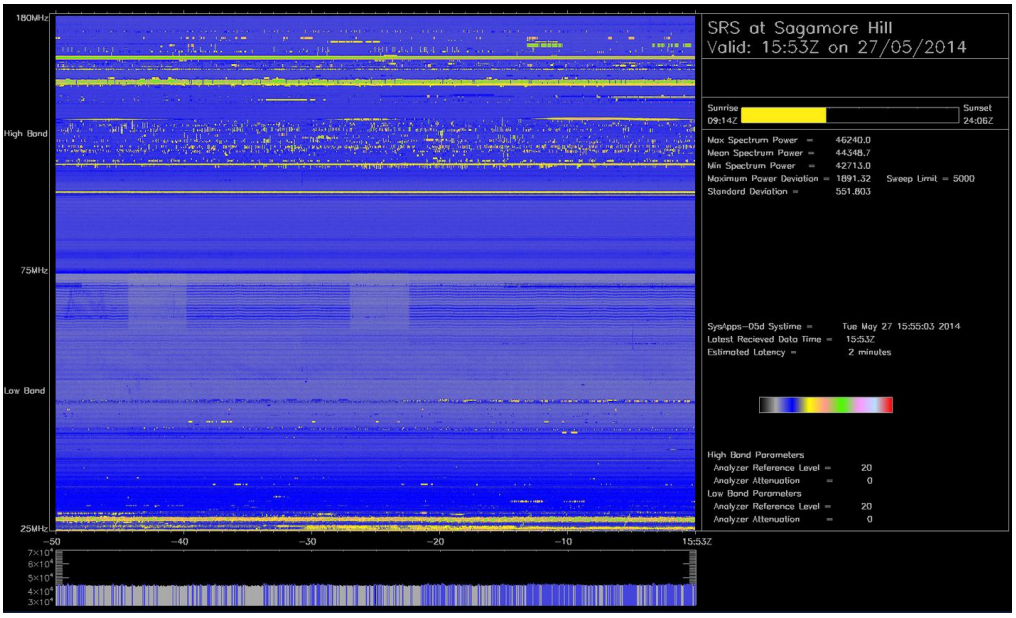

Figure 1. Solar Radio Spectrograph Display

3. AUTOMATED DETECTION OF TYPE III SOLAR RADIO BURSTS

The development of an automated detection and typing algorithm was motivated by the ability to rapidly find solar radio events in archives. Type III radio bursts occur frequently so the database of these events is quite large. This provided fertile ground for the development of an automated algorithm. Figure 2 shows an example of a classic Type III radio burst in the 25-180 MHz frequency band.

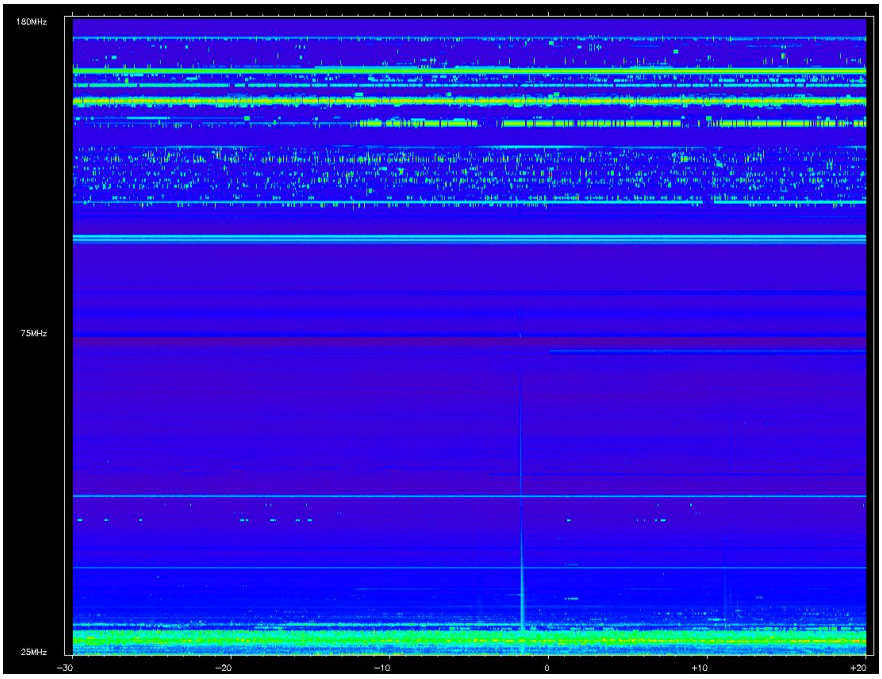

Figure 2. Type III Radio Burst at Sagamore Hill on 3 Dec 2013 at 14:37 UTC.

The method described in this paper for detecting Type III radio bursts takes advantage of mathematical morphology techniques first developed for imagery analysis [9]. Mathematical morphology is based on set theory in which sets represent shapes that are manifested in images. The sets can be of any dimensionality, but in our current algorithm the sets are two-dimensional and operate on binary images. Since the SRS data are presented in three dimensions (time, frequency, and intensity), a preprocessing step employs a directional convolution to detect sharp second-order gradients. The second-order gradients are determined along the time axis to eliminate much of the radio frequency interference generated by Earth-based sources (television stations, satellites, etc.). Details of the algorithm are discussed in the following paragraphs.

The one-minute bundled data files are first checked for their integrity by checking the file size. Any files not identical to the expected file size are exempted from further processing. Next the files are opened, parsed, and oriented into arrays such that frequency is the vertical coordinate, time is the horizontal component and the intensity is the Z- component (represented by color on the display). This yields an array that is 802 rows by 20 columns (802 frequencies by 20 3-sec sweeps).

The intensity array, represented by the function *f*, is subjected to a convolution operator with a kernel, *g*, designed to detect high-intensity short-duration horizontal second-order gradients in the intensity coordinate such that,

$$g = \begin{bmatrix} 1 & -2 & 1 \\ 1 & -2 & 1 \\ 1 & -2 & 1 \end{bmatrix},$$

$$A = [\, f * g](t) = \int_{t1}^{t2} g(\tau)\, f(t-\tau) d\tau,$$

and where $[\, f * g](t)$] denotes the convolution of *f* and *g*.

The result of this operation removes the horizontally-oriented features and highlights the vertically-oriented (across frequency bins) features.

The convolution result is further refined by removing concave up intensities since Type III radio bursts would produce a concave down intensity (low intensity followed by high intensity followed by low intensity). This detects the leading edge of the Type III radio bursts and prevents double counting of the feature by finding the trailing edge.

The result of the convolution is then subjected to morphological transformations with a structuring element B representing the shape parameters of a Type III radio burst. These transformations combine the two sets, *A* and *B*, using vector addition or subtraction. The structuring element is an adjustable parameter in this algorithm that can be used to increase positive identification at the expense of increased false alarms. The structuring element used by the current algorithm is a vertically-oriented vector of 55 elements (corresponding to 55 frequency bins). The size of this vector was empirically-determined from observations of Type III radio bursts. Longer vectors reduce the number of detections but also reduce the number of false alarms.

The first operator applied to the two sets is erosion. This operator combines the two sets in Euclidian N-space (E^N) using vector subtraction of the set elements *a* and *b* of *A* and *B* respectively to produce a new set of elements *x*. The erosion definition is:

$$A \ominus B = \{x \in E^N \mid x + b \in A \text{ for every } b \in B\}.$$

An example of the operator is as follows:

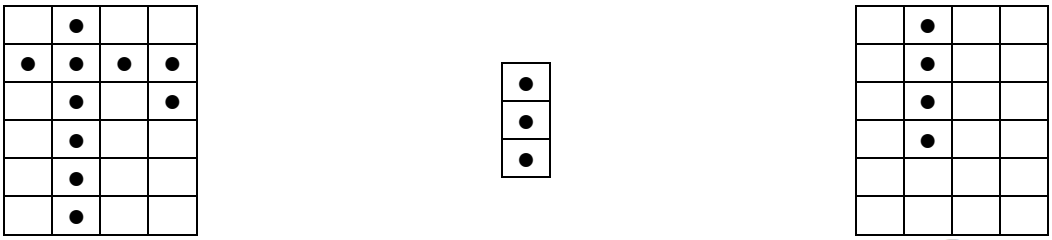

The next morphological operator applied is dilation which is applied to the results of the erosion operator. Dilation is the morphological dual to erosion which combines two sets using vector addition to create a new set of *x* elements. Dilation is defined by:

$$A \oplus B = \{x \in E^N \mid x = a + b \text{ for some } a \in A \text{ and } b \in B\}.$$

An example of the operator applied to the results of the previous erosion example is as follows:

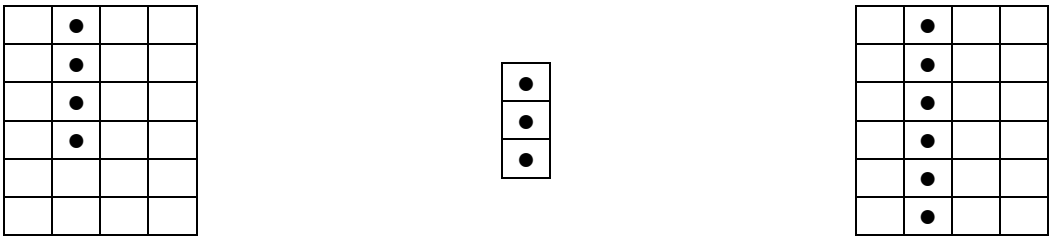

The result of the morphological operators is a binary array that emphasizes the vertical structures in the original set A. This methodology was applied to the SRS data in a validation effort and is described in the following sections.

4. DATA USED IN THIS STUDY

Data were collected from the Sagamore Hill Solar Observatory for the month of December 2013. These data represented the SRS measurements of solar activity at a 3-second cadence during daylight hours for the entire month. Type III reports were extracted from the analyst logs of all reported solar radio bursts and used to validate the algorithm. In addition to the official record, all raw data were manually re-inspected to account for any missed events in the official record. This data set was also used to validate the algorithm.

5. VALIDATION OF ALGORITHM

Validation began by evaluating the raw data with the automated algorithm. All automatically detected Type III events were recorded in log files and compared to the official record. Of the 39 reported by the analysts and verified visually, the algorithm detected 31…a 79.4% hit rate. The eight missed events were inspected to further understand the weakness in the algorithm. These events tended to have very weak intensities and some were also of longer duration than the algorithm considered acceptable. All the Type III's with classic signatures were detected by the algorithm.

However, the algorithm did detect Type III's that were not in the official record. These tended to be very weak intensity Type III's and often embedded in a confused background of anthropogenic radio frequency interference. Oftentimes during the manual inspection, it was difficult to find these weak Type III events with a casual look. However, with the knowledge from the algorithm that the event occurred, all these events were verified. Manual verification revealed the existence of 111 events, many with very weak intensities. The algorithm detected 94 of these events yielding a hit rate of 84.6%. These findings and results are similar to the Lobzin et al. automated detection algorithm using Radon transforms [10].

False alarms were also evaluated. Reexamination of the Type III events reported in the analysts log revealed 8 false alarms. Generally these were related to documentation errors (mistyped times) in the logs. This compares to the automated algorithm discovery of 143 events during this month (recall the manual verification of 111 events). This yields a 28.8% false alarm rate. Generally these false alarms were associated with the onset of broadband anthropogenic radio frequency interference or lightning. This could be reduced by additional algorithms specifically designed to detect these types of events thus providing the ability to override the Type III decision.

6. WAY AHEAD

This algorithm is currently running in real time on the system that displays the SRS data. Further evaluation of the algorithm is ongoing. Additional algorithms will be considered for other types of radio bursts as well as radio frequency interference identification. The various types of signatures will drive different solutions for these typing algorithms.

7. SUMMARY AND CONCLUSIONS

In this paper we described an algorithm for automatically detecting Type III radio bursts. This algorithm implements mathematical morphology techniques to extract features that fit the physical representation of these bursts on solar radio spectrographs. The algorithm was validated against an independent analysis and yielded a 79.4% hit rate. Since the algorithm returned many more hits than the official record manual reanalysis on the raw data was conducted revealing numerous additional (albeit low intensity) events. After validation against these events the algorithm produced a hit rate of 94 out of 111 events (84.6%) and a false alarm rate of 28.8% (143 out of 111 events). The false alarm rate could be reduced with the development of other

automated recognition algorithms to detect sources of anthropogenic and natural radio frequency interference.

8. BIBLIOGRAPHY

1. K. F. Tapping, "The 10.7 cm Solar Radio Flux (F10.7)," Space Weather, vol. 11, pp. 394-406, 2013.
2. J. K. Hargreaves, The Solar Terrestrial Environment, Cambridge: Cambridge University Press, 1995.
3. M. J. Aschwanden, Physics of the Solar Corona: An Introduction, Chichester, UK: Praxis Publishing, 2002.
4. J. A. Kennewell, "Solar Radio Interference to Satellite Downlinks," in Sixth International Conferenece on Antennas and Propagation, Coventry, 1989.
5. J. A. Kennewell and A. McDonald, "GPS Interference By Solar Radio Bursts," Australian Government Bureau of Meteorology, [Online]. Available: http://www.ips.gov.au/Educational/1/3/10. [Accessed May 2014].
6. V. Sreeja, M. Aquino, K. d. Jong and a. H. Visser, "Effect of the 24 September 2011 solar radio burst," Space Weather, vol. 12, pp. 143-147, 2014.
7. D. E. Gary, L. J. Lanzerotti, G. M. Nita and a. D. J. Thomson, "Effects of Solar Radio Bursts on Wireless Systems," NSF Space Weather Program, 2003.
8. J. Ralston, J. Heagy and a. R. Sullivan, "Environmental/Noise Effects on VHF/UHF UWB SAR," Institude for Defense Analyses, Alexandria, VA, 1998.
9. R. M. Haralick, S. R. Sternberg and X. Zhuang, "Image Analysis Using Mathematical Morphology," IEEE Transactions on Pattern Analysis and Machine Intelligence, Vols. PAMI-9, no. 4, pp. 532-550, 1987.
10. V. V. Lobzin, I. H. Cairns, P. A. Robinson, G. Steward and a. G. Patterson, "Automatic Recognition of Type III Solar Radio Bursts: Automated Radio Burst Identification System Method and First Observations," Space Weather, vol. 7, 2009.